Space-time non-separable pulses: Constructing isodiffracting donut pulses from plane waves and single-cycle pulses

Apostolos Zdagkas,[1] Nikitas Papasimakis,[1] Vassili Savinov,[1] and Nikolay I. Zheludev[1,2]

[1] *Optoelectronics Research Centre and Centre for Photonic Metamaterials, University of Southampton, Southampton SO17 1BJ, United Kingdom*

[2] *Centre for Disruptive Photonic Technologies, School of Physical and Mathematical Sciences and The Photonics Institute, Nanyang Technological University, Singapore 637378, Singapore*

(Dated: October 22, 2020)

Abstract

Maxwell's equations can be satisfied not only by plane electromagnetic waves, but also by more exotic space-time non-separable electromagnetic pulses which cannot be represented as a product of time and space dependent functions. A family of such pulses with finite energy was identified by R. Ziolkowski in 1985. Later R. W. Hellwarth and P. Nouchi highlighted a subset of Ziolkowski's pulses, now known as Flying Donuts, a formation of polarization singularities of toroidal topology traveling at the speed of light. Spurred by recent advances in ultrafast and topological optics, space-time non-separable electromagnetic excitations are now becoming the focus of growing experimental efforts as they hold promise for topological information transfer, probing and inducing transient excitations in matter such as anapole and toroidal modes. Many practical questions are yet to be answered regarding their generation, detection and light-matter interactions. Here we demonstrate that the Flying Donut is bandwidth limited and can be constructed from an ensemble of monochromatic plane waves with continuous spatial and frequency spectrum and hence can be generated by converting broadband conventional transverse electromagnetic pulses.

I. INTRODUCTION

Flying Donuts (FDs) are single-cycle pulses with toroidal electromagnetic field configuration and unusual spatio-temporal coupling [1]. FD pulses exhibit a fine topological structure along with regions where energy back-propagation occurs [2], while even their interaction with simple homogeneous media is non-trivial [3]. They form the free-space propagating counterparts of the recently established toroidal excitations in matter, i.e. charge-current configurations with Donut-like topology [4]. In fact, it has been shown that Flying Donut pulses can efficiently engage dynamic toroidal and anapole excitations in dielectric particles, even when the latter does not posses toroidal symmetry [3, 5].

Flying Donuts were introduced in the context of Brittingham's work on "focus wave modes" (1983) where he described a new class of wideband non-diffracting pulses, localized solutions to Maxwell's equations [6]. Soon after, R. W. Ziolkowski showed that, although "focus wave modes" are unphysical and have infinite energy [7], a finite energy pulse can be constructed from superposition of such modes [8]. In fact these finite energy pulses originate from modified Gaussian pulses that emerge as solutions of the scalar wave equation with moving complex sources. An example of such a pulse is the "splash pulse" [9]. In 1996 Hellwarth and Nouchi found special cases of Ziolkowski's solution, space-time non-separable finite energy linearly polarized "pancake"pulses [10, 11] and Flying Donut pulses of toroidal symmetry [1].

Although the generation of electromagnetic and acoustic analogs of localized pulses based on Ziolkowski's solutions has been presented in the literature [12–14], the generation of electromagnetic FDs has not been demonstrated." However, recent works have shown that FD pulses could be generated in the optical part of the spectrum from a laser pulse interacting with appropriately patterned metasurfaces [15, 16]. Here, the generation of FD pulses requires to address simultaneously their few cycle nature, toroidal symmetry and importantly space-time coupling (STC). STCs appear as non-uniform spectral or temporal properties across a plane normal to the propagation vector of a pulse. Although apparent in the time domain, STCs can sometimes be more intuitively studied in the frequency domain as space-spectrum couplings. Evidently, a plane wave expansion is highly desirable for the generation and study of light-matter interactions of FD pulses.

In this work, we provide closed form expressions for the time-frequency Fourier transform

of the pulse. We use the derived analytical expressions to show that the FD does exhibit space-spectrum coupling. In fact, we show that in the paraxial regime the pulse exhibits isodiffracting propagation, i.e. in each cross-section of the beam perpendicular to the direction of propagation the spatial profiles of intensity for every frequency component scale in the same way along the trajectory of the beam. We expect that this type of propagation invariance will be useful for energy transfer applications like free-space communications and micromachining. The frequency domain expressions reported here facilitate the generation and characterization of FDs [15, 16], as well as the study of their interactions with matter through efficient Fourier propagation methods [17]. In addition, we present a simple expression for the spatial Hankel transform that reveals the focusing properties of FDs and leads to a semi-analytical plane wave expansion of the pulse. The latter is used to reveal hidden features of the pulse, such as the role of back-propagating plane waves in the non-paraxial regime and it provides an insight on how the simplest form of linear polarized electromagnetic waves can be combined to generate a pulse with complex spatiotemporal and vectorial structure.

II. TIME-FREQUENCY FOURIER TRANSFORM OF THE FLYING DONUT

The Flying Donut pulse can exist in transverse electric (TE) and transverse magnetic (TM) field configurations. In the TE case, the electric field is azimuthally polarized, whereas the magnetic is longitudinally and radially oriented. The TM pulse can be derived from the TE by exchanging the electric and magnetic fields as follows

$$\mathbf{E}_{\mathrm{TM}} = \sqrt{\frac{\mu_0}{\epsilon_0}}\mathbf{H}_{\mathrm{TE}} \tag{1}$$

$$\mathbf{H}_{\mathrm{TM}} = -\sqrt{\frac{\epsilon_0}{\mu_0}}\mathbf{E}_{\mathrm{TE}} \tag{2}$$

and describes a radially polarized FD.

The FD pulse itself emerges from a scalar "seed function" [1]

$$f\left(t,\,\mathbf{r}\right) = f\left(t,\,\rho,z\right) = \frac{1}{\rho^2 - \left(\left(ct-z\right)+iq_1\right)\left(\left(ct+z\right)+iq_2\right)} \tag{3}$$

which is a solution of the scalar wave equation. Here, ρ and z are the radial and longitudinal

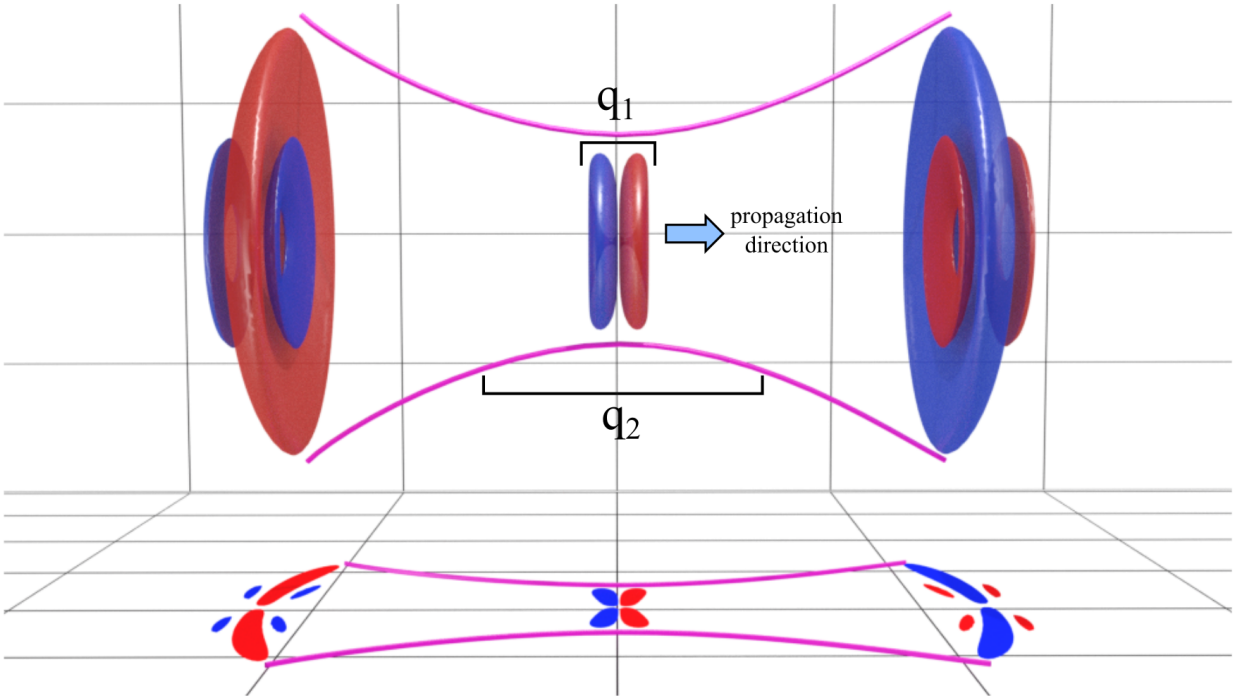

FIG. 1. Propagation of the single-cycle TE FD pulse. Owing to the Gouy phase shift, a "$1\frac{1}{2}$-cycle" pulse (left) transforms into a "1-cycle" pulse at focus (center), and resumes its "$1\frac{1}{2}$-cycle" duration after propagating through the focal region (right). The fact that the pulse acquires a π phase by travelling through the focus is also shown from the phase of the electric field where the blue and red colors before and after focus are exchanged.

coordinates, t is the time, c is the speed of light in vacuum while q_1 and q_2 are free parameters that, as will become apparent later in the text, define the central frequency and the focusing strength of the pulse respectively. In a cylindrical coordinate system the electric ($\mathbf{E}$) and magnetic ($\mathbf{B}$) fields of the TE FD pulse are derived from the following equations [1, 18]

$$
\begin{aligned}
E_\theta &= \mu_0 \partial_t \partial_\rho f \\
B_\rho &= \mu_0 \partial_z \partial_\rho f, \\
B_z &= \mu_0 \left(\partial_z^2 f - \frac{1}{c^2} \partial_t^2 f \right)
\end{aligned}
$$

where $\partial_t, \partial_\rho, \partial_z$ are the partial derivatives with respect to t, ρ and z.

The azimuthally polarized TE FD pulse can therefore be presented as [10]:

$$E_\theta = -4\mathrm{i}f_0\sqrt{\frac{\mu_0}{\epsilon_0}}\frac{\rho\left(q_1+q_2-2\mathrm{i}ct\right)}{\left[\rho^2+(q_1+\mathrm{i}\tau)(q_2-\mathrm{i}\sigma)\right]^3} \tag{4}$$

$$H_\rho = 4\mathrm{i}f_0\frac{\rho\left(q_2-q_1-2\mathrm{i}z\right)}{\left[\rho^2+(q_1+\mathrm{i}\tau)(q_2-\mathrm{i}\sigma)\right]^3} \tag{5}$$

$$H_z = -4f_0\frac{\rho^2-(q_1+\mathrm{i}\tau)(q_2-\mathrm{i}\sigma)}{\left[\rho^2+(q_1+\mathrm{i}\tau)(q_2-\mathrm{i}\sigma)\right]^3}, \tag{6}$$

where ϵ_0 and μ_0 are the vacuum permittivity and permeability respectively, $\tau = z - ct$, $\sigma = z + ct$ and f_0 a constant defining the amplitude and the units. The pulse is defined by q_1 and q_2 and from now on we assume that $q_1 \leq q_2$. When compared to a Gaussian beam, q_1 has the role of the wavelength and q_2 the role of the Rayleigh length. Similarly to Gaussian pulses, FD pulses can be focused. Both real and imaginary parts are solutions to Maxwell's equations, termed here "1-cycle" and"$1\frac{1}{2}$-cycle", respectively, reflecting their duration at focus, see Fig. 2a-b. Owing to Gouy phase shifts, the shape of the pulse at focus is different from that in the far-field [10] with the real (imaginary) part transforming from "$1\frac{1}{2}$-cycle" ("1-cycle") away from focus to a "1-cycle" pulse ("$1\frac{1}{2}$-cycle") at focus (see Fig. 1).

To date, exact closed-form expressions for the FD pulse have only been defined in the time domain. Although the time domain expressions Eqs. 4-6 allow to describe the FD pulse in a compact fashion, frequency domain expressions are crucial for generating and understanding the propagation dynamics of FDs. We have derived analytically such expressions for both the real and imaginary parts of the TE and TM pulses (see Appendix A). Here, we focus on the real part of the TE FD pulse (the "1-cycle" azimuthally polarized pulse):

$$E_{\mathrm{re}}(\omega) = \begin{cases} 4f_0\sqrt{\mu_0/\epsilon_0}\left\{\mathrm{i}\pi\frac{\omega}{c^2}\frac{\rho}{q_1}e^{-\frac{\omega(q_2+q_1)}{2c}}\frac{e^{\frac{\mathrm{i}\omega}{2c}\sqrt{A}}\left(2\mathrm{c}\mathrm{i}+\omega\sqrt{A}\right)+e^{-\frac{\mathrm{i}\omega}{2c}\sqrt{A}}\left(-2\mathrm{c}\mathrm{i}+\omega\sqrt{A}\right)}{2A^{3/2}}\right\}^* & \omega > 0 \\ 4f_0\sqrt{\mu_0/\epsilon_0}\mathrm{i}\pi\frac{\omega}{c^2}\frac{\rho}{q_1}e^{\frac{\omega(q_2+q_1)}{2c}}\frac{e^{-\frac{\omega\mathrm{i}}{2c}\sqrt{A}}\left(-2\mathrm{c}\mathrm{i}+\omega\sqrt{A}\right)+e^{\frac{\omega\mathrm{i}}{2c}\sqrt{A}}\left(2\mathrm{c}\mathrm{i}+\omega\sqrt{A}\right)}{2A^{3/2}} & \omega < 0 \\ 0 & \omega = 0 \end{cases} \tag{7}$$

with

$$A \equiv A(\rho, z, q_2) = -(-q_1+q_2-2\rho-2\mathrm{i}z)(-q_1+q_2+2\rho-2\mathrm{i}z). \tag{8}$$

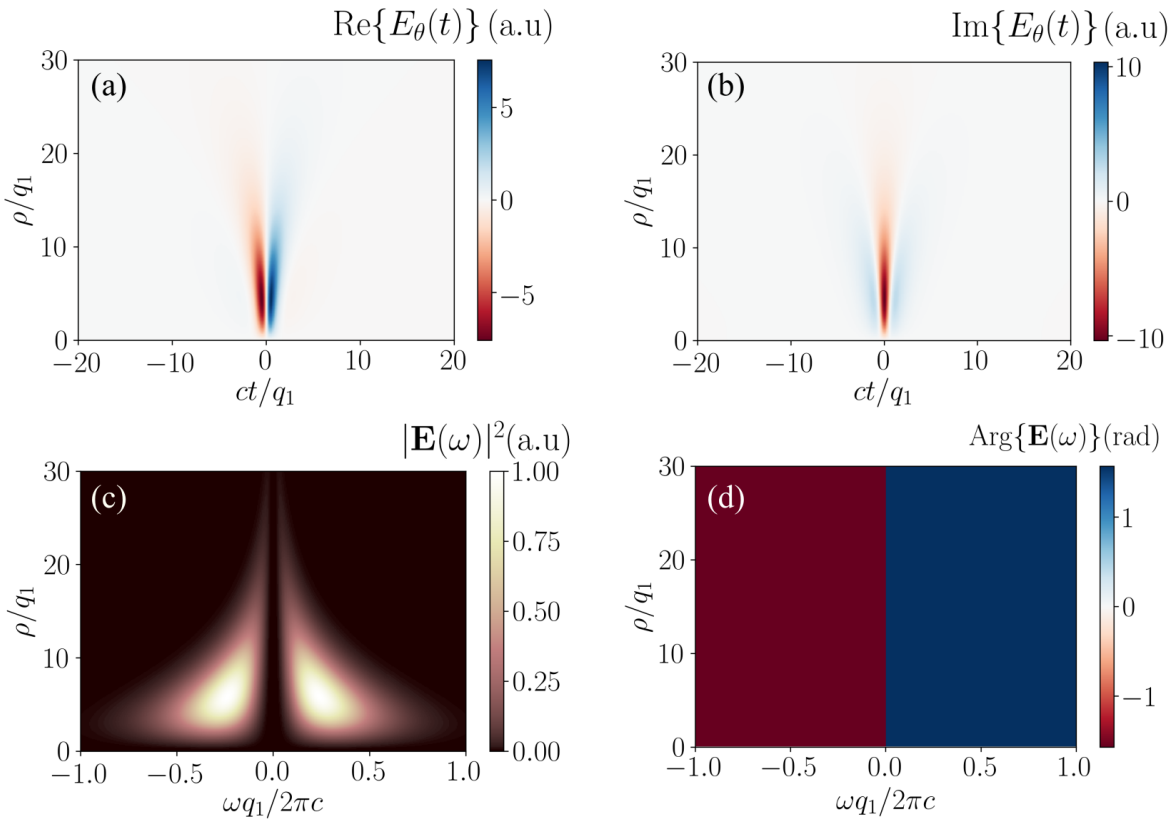

FIG. 2. (a-b) Time-radius cross sections of the electric field of the "1-cycle" and "$1\frac{1}{2}$-cycle" TE pulses respectively at their focus for $q_2 = 100q_1$. (c-d) Radial distribution of spectral power (c) and spectral phase (d) of the TE "1-cycle" pulse.

Equation 7 allows us to examine the spectral phase of the FD pulse. From Eq. 8 one can see that at focus $\sqrt{A}$ is either real, $\rho \geq (q_2 - q_1)/2$, or imaginary $\rho < (q_2 - q_1)/2$, and in both cases it leads to an imaginary field in the frequency domain for any radius. Since the field has flat spectral phase $\theta(\rho, \omega) = \pm\pi/2$ (see Fig. 2d), the pulse described by Eqs. 4-6 is bandwidth limited. Away from the focus, the spectral phase has terms exponential on $\omega\sqrt{A}$, and since A is a quadratic function of ρ, these terms are non-separable functions of frequency ω and coordinate ρ.

In Fig. 2c, we plot the radial distribution of spectral power of the pulse at focus, $z = 0$, where the space-frequency coupling becomes apparent. The spectrum is broad at the central part of the pulse and narrows towards the peripheral parts, where lower frequency components are prominent. This distribution of frequencies is invariant upon propagation indicating that the FD is very close to an ideal isodiffracting pulse. Indeed, isodiffracting pulses have spatial profiles of intensity for every frequency component that scale along the

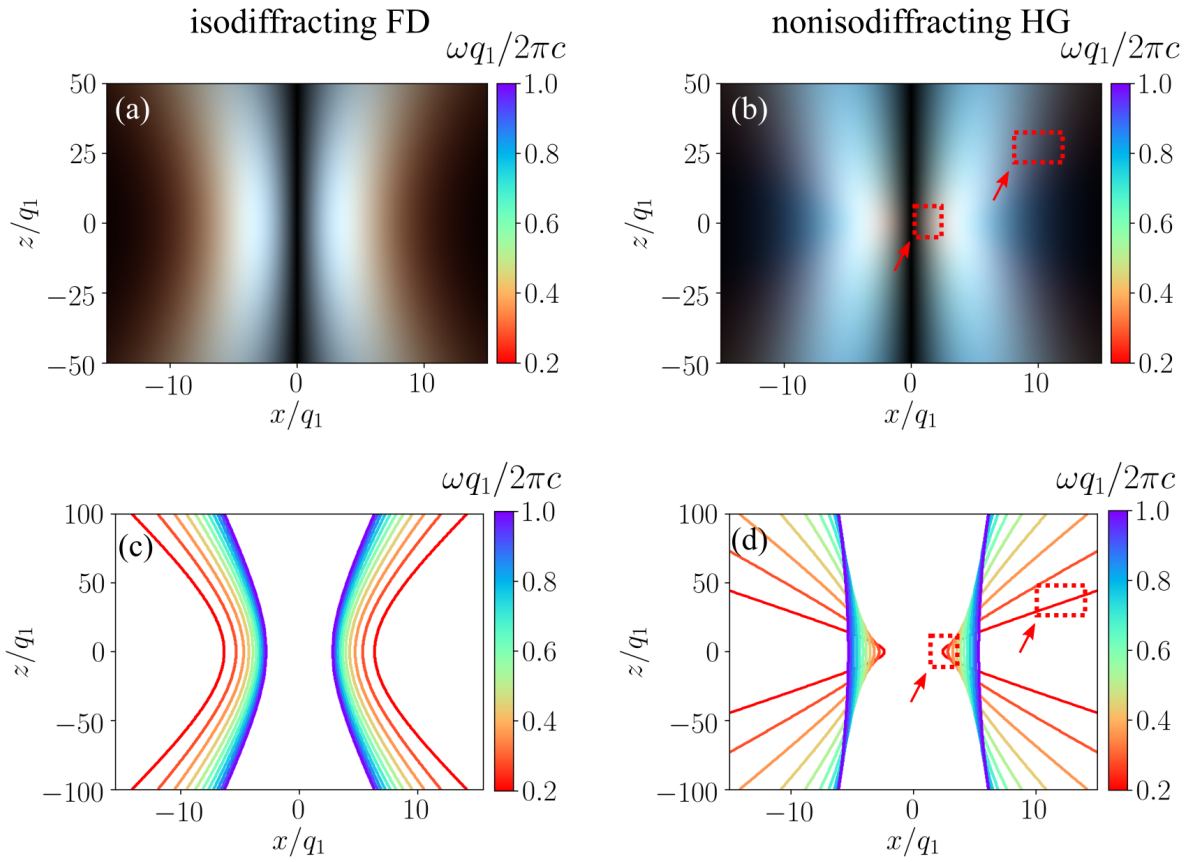

FIG. 3. (a-b) False color representation of $x-z$ cross sections at $y/q_1 = 0$ of the electric field intensity of the spectral components of the isodiffracting FD pulse and if a nonisodiffracting Hermite-Gauss beam respectively. The range of presented frequency components spans the full bandwidth of the FD pulse. The brightness represents the intensity distribution in space while color corresponds to the different wavelengths. Blue and red colors present shorter and longer wavelengths, respectively. (c-d) Traces of the position of the maximum intensity for each wavelength for the FD (c) and a nonisodiffracting Hermite-Gauss beam (d). While the maxima of the different wavelengths of the FD pulse do not mix, the nonisodiffracting Hermite-Gauss spectral components mix at focus with the longer wavelengths being tightly focused and hence later being strongly diffracted (see areas highlighted by the red squares in (b) and (d)).

trajectory of the pulse in the same way. The isodiffracting nature of FD becomes clear in Fig. 3 where the FD and a nonisodiffracting pulse composed of Hermite-Gauss beams are compared. A false color image made of all the composing frequencies of the pulse and a plot with the trace of the position of the maximum intensity for each frequency are plotted. The isodiffracting nature of the FD leads to a separation of the wavelengths with the maxima of the longer wavelengths located at larger radii and the shorter wavelengths closer to the center at any propagation distance, as it is also shown in Fig. 2c. In contrast, in

the nonisodiffracting Hermite-gauss pulse the maxima of the longer wavelengths are strongly focused resulting in different lateral spectral profiles for different propagation distances. The isodiffracting nature of the FD pulse can be rigorously derived in the case of well collimated pulses ($q_2 \gg q_1$), (see Appendix B).

III. SPATIAL HANKEL TRANSFORM OF THE FLYING DONUT

Owing to its toroidal field configuration, the FD pulse is rotationally symmetric and thus can be expanded in cylindrically symmetric single-cycle pulses by virtue of the Hankel transform [17]. The Hankel transform of the electric field for the TE pulse can be derived as (see Appendix C)

$$\mathbf{E}_\theta(k_\rho) = -\pi f_0 \sqrt{\frac{\mu_0}{\epsilon_0}}(q_1 + q_2 - 2\mathrm{i}ct)\frac{k_\rho^2}{\alpha}K_1(k_\rho\alpha)\hat{\boldsymbol{\theta}}, \tag{9}$$

with $\alpha = \sqrt{(q_1 + \mathrm{i}z - \mathrm{i}ct)(q_2 - \mathrm{i}z - \mathrm{i}ct)}$ and K_1 the first order modified Bessel function of the second kind. The transforms of the real and imaginary parts, or the "1-cycle" and "$1\frac{1}{2}$-cycle", are given by

$$E_{\mathrm{re},\theta}(k_\rho) = \frac{E_\theta(k_\rho) - E_\theta^*(k_\rho)}{2} \tag{10}$$

$$E_{\mathrm{im},\theta}(k_\rho) = \frac{E_\theta(k_\rho) + E_\theta^*(k_\rho)}{2\mathrm{i}}, \tag{11}$$

respectively.

The closed form expression is a well behaved function in contrast to the numerical Hankel transform that is inaccurate close to the axis of symmetry [19]. It also simplifies the study of the pulse in momentum space which provides information about its focusing properties. Figure 4 shows the electric field Hankel transforms of the "1-cycle" (Fig. 4a-b), and "$1\frac{1}{2}$-cycle" (Fig. 4d-e) pulses at focus ($t = 0$) for $q_2 = 100q_1$. The former is antisymmetric with respect to the z coordinate and vanishes at $z = 0$ and $t = 0$ (see Fig. 4c). On the other hand, the Hankel transform of the "$1\frac{1}{2}$-cycle" pulse is symmetric with respect to z and peaks at $z = 0$.

The Hankel transform decomposes the FD pulse into a set of pulses with different focusing strengths. As a result, Fig. 4c and f illustrate that the FD is composed out of weakly

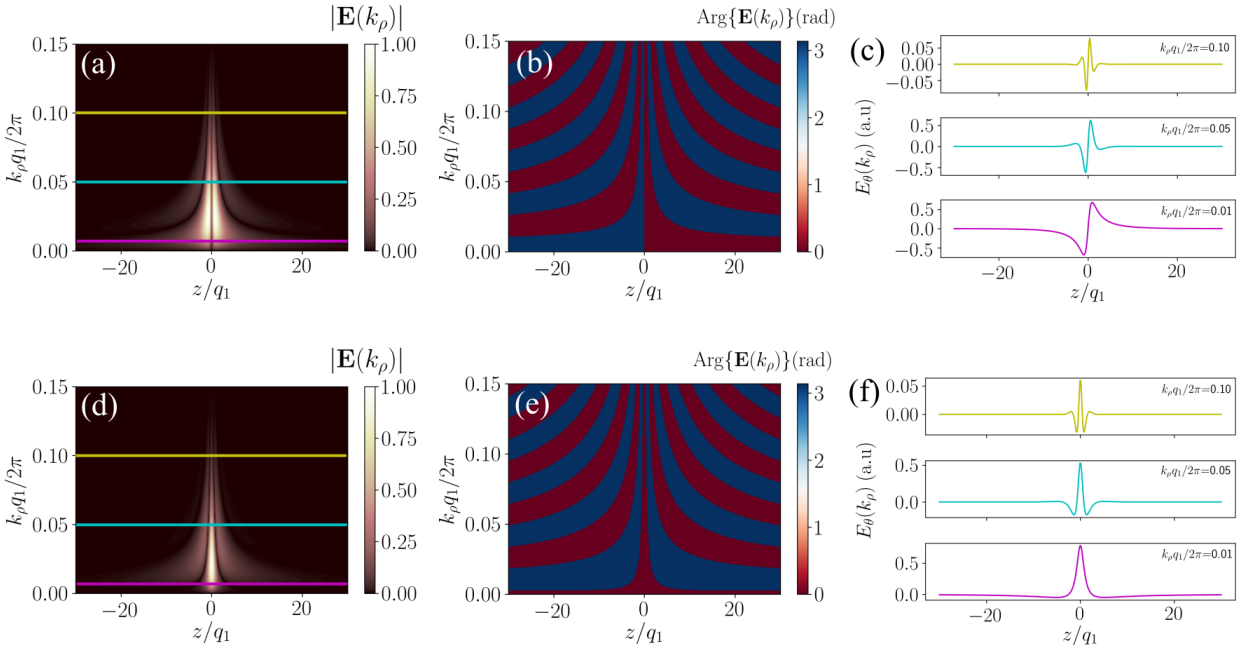

FIG. 4. Amplitude and phase of the Hankel transforms of the "1-cycle", (a) and (b), and "$1\frac{1}{2}$-cycle", (d) and (e), electric fields at focus, $t = 0$, and for $q_2 = 100q_1$. (c) and (f) The imaginary part of the Hankel transform of the "1-cycle" and "$1\frac{1}{2}$-cycle" pulses at three different values of k_ρ.

focused (low k_ρ) single cycle pulses (magenta coloured line) and strongly focused (high k_ρ) blue-shifted broader pulses (yellow line). It exhibits a flat radial spectral phase profile at $z = 0$ (Fig. 4b and e) indicating that at focus the FD pulse can be decomposed in a set of in-phase cylindrically symmetric pulses. Away from focus the sign of the phase alternates with increasing spatial frequency, a trait which is related to the isodiffracting nature and fine topological structure of the pulse [2].

IV. PLANE WAVE EXPANSION OF THE FLYING DONUT PULSE

The Hankel transform allows to readily expand the FD pulse into plane waves. Indeed, for the plane wave expansion of the FD pulse, two spatial ($(\rho, z) \to (k_\rho, k_z)$) and one temporal ($t \to \omega$) transform is required, of which only one at a time can be derived analytically (either time-frequency Fourier or Hankel transform). Since the radial transform is given by a simple analytical expression, the Fourier transform of the two remaining dimensions, time and longitudinal position, can be easily performed numerically. The result of the plane wave decomposition is presented in Fig. 5 for three different cases, $q_2 = 2q_1$, $q_2 = 10q_1$ and

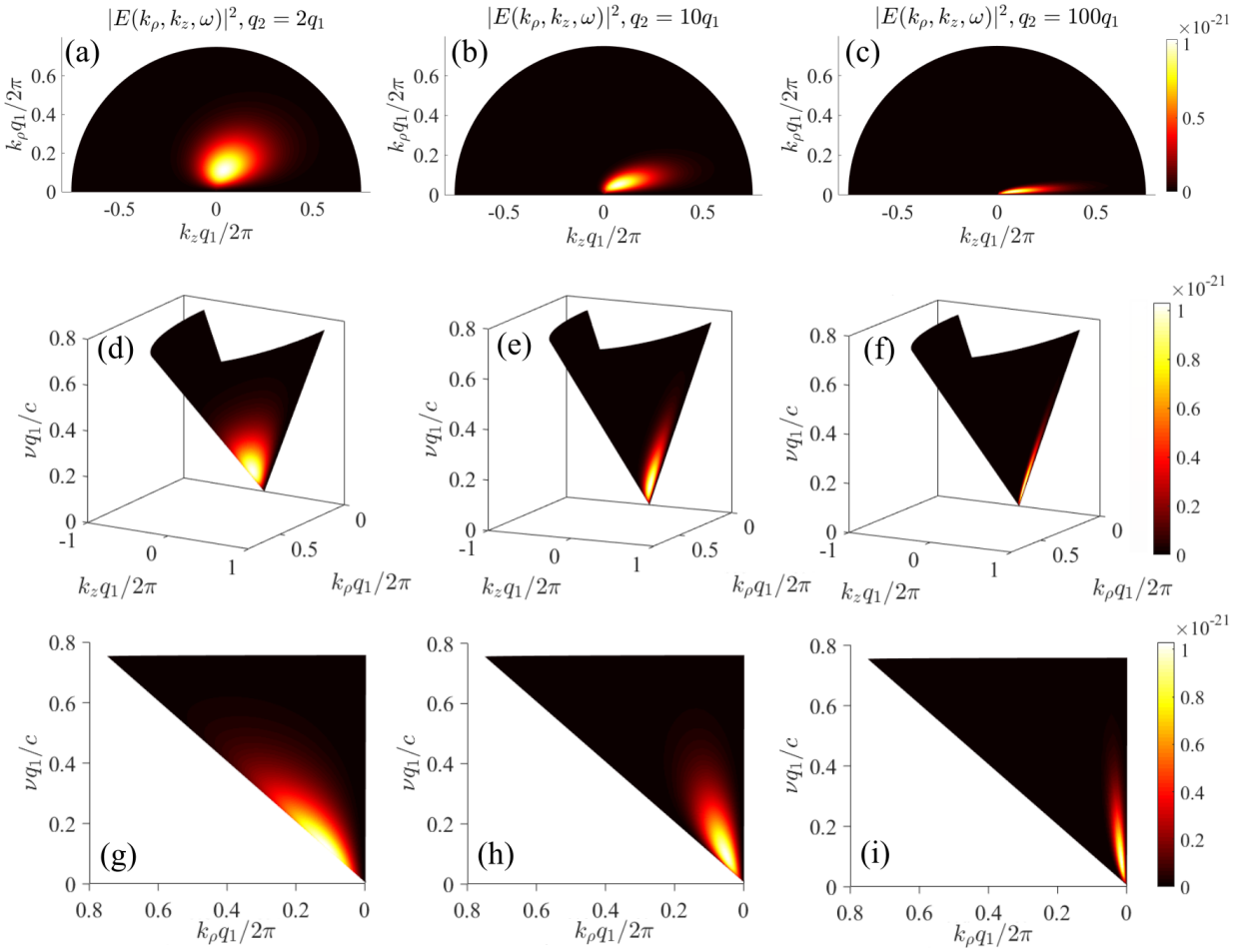

FIG. 5. Plane wave decomposition of the FD pulse presented on the surface of a half-cone, representing the cone of light ($\omega = ck$). (a-c) The $k_\rho - k_z$ projection of the decomposition. (d-f) Full three-dimensional presentation of the plane wave spectrum on the light cone. (g-i) The $\nu - k_\rho$ projection of the decomposition. The colors represent the squared electric field amplitude of the plane waves in arbitrary units. Only positive frequencies are considered.

$q_2 = 100q_1$. The decomposition is given at the surface of a cone that represents the cone of light (defined by $\omega = c|k|$). Only positive k_ρ are presented since the pulse is azimuthally symmetric. The first row depicts the projection of that cone to the $k_\rho - k_z$ plane, the third row depicts the projection in the frequency-radial spatial frequency, $\nu - k_\rho$, plane while in the middle row a 3D view of the plane wave expansion is presented. The colors represent the squared amplitude of the plane wave components. The plot is given only for positive frequencies.

Figure 5a indicates that in the extreme non-paraxial regime, where $q_2 \simeq q_1$, backward propagating waves are present in the FD pulse. This is revealed by the appearance of

negative k_z for positive frequencies. However, by increasing q_2 with respect to q_1, we notice that the contribution of backward propagating waves rapidly vanishes. Moreover, we observe a decrease of k_ρ in favour of k_z, indicating that the pulse is weakly focused and hence it propagates as a paraxial pulse ($q_2 \gg q_1$). The existence of forward and backward propagating waves emanates from Eq. 3 as discussed in [8, 20]. The space-time non-separability reveals itself in the $\mathbf{k} - \omega$ domain, where low (high) frequencies correspond to small (large) range of radial wavevectors indicating that they are weakly (strongly) confined in the transverse plane. In addition, we note that small (large) radial wavevectors k_ρ, are accompanied by a narrower (broader) bandwidth, as is evident in Fig. 5h. This behaviour is in accordance with the isodiffracting nature of the FD pulse (see also discussion in Sec. II).

The presented decomposition of the pulse into plane waves illustrates how the simplest form of electromagnetic waves with linear polarization can be combined to generate a pulse with complex spatiotemporal and vectorial structure. Previous analysis of localized waves, in particular "focus wave modes", has highlighted the importance of considering the description and generation of space-time coupled pulses in the frequency domain [21, 22]. In these works, plane waves whose amplitude is described by a non-separable equation in $\mathbf{k} - \omega$ space can be combined to form space-time coupled solutions of the scalar wave equation. A weighted superposition of such waves also results in a space-time coupled solution. In a similar manner, the plane wave expansion of the FD provides an invaluable tool for the study of its propagation dynamics and light-matter interactions and will inform the development and implementation of generation and detection schemes for FD pulses.

V. SUMMARY

In this paper we have presented a series of decompositions of the FD pulse. We have derived closed form expressions for the Fourier transform and provided a frequency domain description of the FD pulse. The Fourier transform expression indicates that the FD pulse is space-spectrum non-separable and in fact very close to an ideal isodiffracting pulse, a property that ensures the preservation of its spectral profile upon propagation. In addition, the Fourier decomposition of the pulse into monochromatic beams facilitates the study of its propagation properties by enabling the use of efficient frequency domain propagation techniques [17]. Moreover, such a decomposition can be used not only for the study of the

pulse propagation dynamics, but also, for the description of the interaction of the FD pulse with matter. The Hankel transform derived here allows to describe the radial spectrum in momentum space and hence reveals information related to the focusing properties of the pulse. It can provide an accurate picture of the spatial frequency distribution of the pulse and hence allows for the decomposition of FDs into plane waves. The plane wave expansion reveals the properties of the complex FD pulse by breaking it down to simple linearly polarized waves. It provides a complementary representation to the time domain one and can reveal properties, such as the degree of focusing of the FD pulse and the existence of backwards propagating waves in the strongly non-paraxial regime.

The spatio-temporal description of FDs in different representations provides a framework for the generation, detection, and study of light-matter interactions of such complex pulses. Pulses whose spatio-spectral profile does not change upon propagation could be important in all applications involving pulsed energy transfer, such as free-space telecommunications, spectroscopy, and manufacturing by light.

ACKNOWLEDGMENTS

The authors acknowledge the support of the MOE Singapore (MOE2016-T3-1-006), the UK's Engineering and Physical Sciences Research Council (grant EP/M009122/1), the European Research Council (Advanced grant FLEET-786851), and the Defense Advanced Research Projects Agency (DARPA) under the Nascent Light Matter Interactions program. We thank the anonymous reviewer for indicating an alternative route to calculate the Hankel transform of Appendix C. The data from this paper can be obtained from the University of Southampton ePrints research repository: https://doi.org/10.5258/SOTON/XXXXX.

Appendix A: Fourier transform

In this appendix a step by step derivation of an analytical expression for the time-frequency Fourier transform of the FD pulse is presented. The following Fourier transform

pair is used

$$\mathbf{F}\left(\mathbf{r},\omega\right)=\int_{-\infty}^{\infty}\mathrm{e}^{\mathrm{i}\omega t}\mathbf{F}\left(\mathbf{r},t\right)dt \tag{A1}$$

$$\mathbf{F}\left(\mathbf{r},t\right)=\frac{1}{2\pi}\int_{-\infty}^{\infty}\mathrm{e}^{-\mathrm{i}\omega t}\mathbf{F}\left(\mathbf{r},\omega\right)d\omega. \tag{A2}$$

For the transverse electric field (TE) we have [1]

$$E_{\theta}=-4\mathrm{i}f_{0}\sqrt{\frac{\mu_{0}}{\epsilon_{0}}}\frac{\rho\left(q_{1}+q_{2}-2\mathrm{i}ct\right)}{\left[\rho^{2}+(q_{1}+\mathrm{i}\tau)(q_{2}-\mathrm{i}\sigma)\right]^{3}} \tag{A3}$$

$$H_{\rho}=4\mathrm{i}f_{0}\frac{\rho\left(q_{2}-q_{1}-2\mathrm{i}z\right)}{\left[\rho^{2}+(q_{1}+\mathrm{i}\tau)(q_{2}-\mathrm{i}\sigma)\right]^{3}} \tag{A4}$$

$$H_{z}=-4f_{0}\frac{\rho^{2}-(q_{1}+\mathrm{i}\tau)(q_{2}-\mathrm{i}\sigma)}{\left[\rho^{2}+(q_{1}+\mathrm{i}\tau)(q_{2}-\mathrm{i}\sigma)\right]^{3}}, \tag{A5}$$

with $\tau=z-ct$ and $\sigma=z+ct$. For convenience and generality, we will use dimensionless variables. More specifically, we write everything with respect to q_1 which has dimensions of length. As such, we define $\rho'=\rho/q_1$, $z'=z/q_1$, $q_2'=q_2/q_1$, $t'=ct/q_1$ and $\omega'=q_1\omega/c$ and we omit the coefficients $4f_0\sqrt{\mu_0/\epsilon_0}/q_1^4$ and $4f_0/q_1^4$ for the electric and the magnetic fields respectively. Finally, we omit the primes on the new dimensionless variables for clarity. Now, the dimensionless fields are given by the following equations

$$E_{\theta}=-\mathrm{i}\frac{\rho(1+q_{2}-2\mathrm{i}t)}{\left[\rho^{2}+(1+\mathrm{i}z-\mathrm{i}t)(q_{2}-\mathrm{i}z-\mathrm{i}t)\right]^{3}} \tag{A6}$$

$$H_{\rho}=\mathrm{i}\frac{\rho(q_{2}-1-2\mathrm{i}z)}{\left[\rho^{2}+(1+\mathrm{i}z-\mathrm{i}t)(q_{2}-\mathrm{i}z-\mathrm{i}t)\right]^{3}} \tag{A7}$$

$$H_{z}=-\frac{\rho^{2}-(1+\mathrm{i}z-\mathrm{i}t)(q_{2}-\mathrm{i}z-\mathrm{i}t)}{\left[\rho^{2}+(1+\mathrm{i}z-\mathrm{i}t)(q_{2}-\mathrm{i}z-\mathrm{i}t)\right]^{3}}. \tag{A8}$$

We will first work with the electric field. From now on and for clarity we will refer to the electric field as E, but we actually mean that we are using the θ component. The real and imaginary parts of the field are quite complex expressions to compute the Fourier integral. Thus, and because of the linearity of the integral operator, we will calculate the Fourier transform of the complex field and then we will take the real and imaginary parts from the

equations,

$$E_{\mathrm{re}}(\omega) = \frac{E(\omega) + E^*(-\omega)}{2} \tag{A9}$$

and

$$E_{\mathrm{im}}(\omega) = \frac{E(\omega) - E^*(-\omega)}{2\mathrm{i}}. \tag{A10}$$

Proof.

$$\begin{aligned} E_{\mathrm{re}}(\omega) &= \int_{-\infty}^{+\infty} e^{\mathrm{i}\omega t}\mathrm{Re}\left\{E(t)\right\} dt \\ &= \int_{-\infty}^{+\infty} \frac{e^{\mathrm{i}\omega t}E(t) + [e^{-\mathrm{i}\omega t}E(t)]^*}{2} dt \\ &= \frac{E(\omega) + E^*(-\omega)}{2}. \end{aligned}$$

□

These correspond to the "1-cycle" and "$1\frac{1}{2}$-cycle" respectively.

Returning now to the equation A6, it is apparent that we can apply Jordan's lemma since the power of t on the denominator is 5 times bigger than that of the numerator. Thus, the Fourier transform is given by the integral residues on the upper and lower half complex plane [23]. One only has to find the poles and determine when they are located in upper half or lower half plane.

From A6, it is apparent that the equation has 2 triple poles, thus only two distinct. Luckily, they are both located in the lower half plane, though the algebra to prove this is elaborate. We are going to prove this explicitly, though a smart way to prove it can be found on [11].

We start by writing down the poles

$$t_1 = \frac{1}{2}\left(\sqrt{-(-1+q_2-2\rho-2\mathrm{i}z)(-1+q_2+2\rho-2\mathrm{i}z)} - \mathrm{i}q_2 - \mathrm{i}\right) \tag{A11}$$

$$t_2 = \frac{1}{2}\left(-\sqrt{-(-1+q_2-2\rho-2\mathrm{i}z)(-1+q_2+2\rho-2\mathrm{i}z)} - \mathrm{i}q_2 - \mathrm{i}\right). \tag{A12}$$

It is useful here to define

$$\begin{aligned} A \equiv A(\rho, z, q_2) &= -(-1 + q_2 - 2\rho - 2\mathrm{i}z)(-1 + q_2 + 2\rho - 2\mathrm{i}z) \\ &= 4z^2 + 4\rho^2 - (q_2 - 1)^2 + 4(q_2 - 1)z\mathrm{i}. \end{aligned} \tag{A13}$$

Now we want to prove that

$$\begin{aligned} \mathrm{Im}\left\{\begin{array}{c} t_1 \\ t_2 \end{array}\right\} = &\frac{1}{2}\Big\{-1 - q_2 \pm \left[(4z - 4zq_2)^2 + (4\rho^2 + 4z^2 - (q_2 - 1)^2)^2\right]^{1/4} \\ &\sin\left[\frac{1}{2}\mathrm{Arg}(A)\right]\Big\} \end{aligned} \tag{A14}$$

is negative for every $q_2 \geq 1, \rho \geq 0$ and z. We will prove it for t_1.

Proof.

$$\mathrm{Arg}(x + \mathrm{i}y) = \mathrm{atan2}(y, x) = \begin{cases} \arctan\left(\frac{y}{x}\right) & x > 0 \\ \arctan\left(\frac{y}{x}\right) + \pi & x < 0 \text{ and } y \geq 0 \\ \arctan\left(\frac{y}{x}\right) - \pi & x < 0 \text{ and } y < 0 \\ +\frac{\pi}{2} & x = 0 \text{ and } y > 0 \\ -\frac{\pi}{2} & x = 0 \text{ and } y < 0 \\ \text{undefined} & x = 0 \text{ and } y = 0. \end{cases} \tag{A15}$$

- For $q_2 = 1$ or $z = 0$, it is immediately apparent from A11 that $\mathrm{Im}\{t_1\} < 0$.
- For $z < 0$, $\mathrm{Arg}(A) < 0$ and thus $\mathrm{Im}\{t_1\} < 0$.
- For $z > 0$, we make use of the trigonometric identity $\sin(\arctan(x)) = \frac{x}{1+x^2}$ and some other more common identities. It can be shown that all the remaining cases

  - $4z^2 + 4\rho^2 - (q_2 - 1)^2 > 0$
  - $4z^2 + 4\rho^2 - (q_2 - 1)^2 < 0$
  - $4z^2 + 4\rho^2 - (q_2 - 1)^2 = 0$

  give $\mathrm{Im}\{t_1\} < 0$.

□

A similar analysis holds for the second pole as well. Knowing that the poles are located in the lower half complex plane, the integral can be calculated from the integral residues

$$\int_{-\infty}^{+\infty} e^{\mathrm{i}\omega t} E(t) dt = 2\pi \mathrm{i} \sum_i \mathrm{Res}\left\{e^{\mathrm{i}\omega t} E(t), t_i\right\} I, \tag{A16}$$

with I denoting the sign of the contour (positive for anticlockwise). In general we have

$$E(\omega) = -2\pi \mathrm{i} \left(\mathrm{Res}\left\{e^{\mathrm{i}\omega t} E(t), t_1\right\} + \mathrm{Res}\left\{e^{\mathrm{i}\omega t} E(t), t_2\right\}\right), \tag{A17}$$

and from A9, the following cases arise

- $(\omega > 0)$

$$E(\omega) = 0 \tag{A18}$$

$$E^*(-\omega) = \left(-2\pi \mathrm{i} \left(\mathrm{Res}\left\{e^{-\mathrm{i}\omega t} E(t), t_1\right\} + \mathrm{Res}\left\{e^{-\mathrm{i}\omega t} E(t), t_2\right\}\right)\right)^* \tag{A19}$$

- $(\omega < 0)$

$$E(\omega) = -2\pi \mathrm{i} \left(\mathrm{Res}\left\{e^{\mathrm{i}\omega t} E(t), t_1\right\} + \mathrm{Res}\left\{e^{\mathrm{i}\omega t} E(t), t_2\right\}\right) \tag{A20}$$

$$E^*(-\omega) = 0. \tag{A21}$$

There are no poles in the upper half plane, but reversal of the sign of ω is equivalent to integrating over the path of the lower half plane. It is advisable to calculate the residues for higher order poles (triple in our case) using a computer algebra system (like Mathematica) in order to avoid mistakes in the trivial but error-prone procedure of computing the derivatives.

Finally the residues are

$$\mathrm{Res}\left\{e^{\mathrm{i}\omega t}E(t),t_1\right\} = -\frac{e^{\frac{\omega}{2}\left(1+q_2+\mathrm{i}\sqrt{A}\right)}\omega\rho\left(2\mathrm{i}+\omega\sqrt{A}\right)}{2A^{3/2}} \tag{A22}$$

$$\mathrm{Res}\left\{e^{\mathrm{i}\omega t}E(t),t_2\right\} = -\frac{e^{\frac{\omega}{2}\left(1+q_2-\mathrm{i}\sqrt{A}\right)}\omega\rho\left(-2\mathrm{i}+\omega\sqrt{A}\right)}{2A^{3/2}} \tag{A23}$$

$$\mathrm{Res}\left\{e^{-\mathrm{i}\omega t}E(t),t_1\right\} = -\frac{e^{-\frac{\omega}{2}\left(1+q_2+\mathrm{i}\sqrt{A}\right)}\omega\rho\left(-2\mathrm{i}+\omega\sqrt{A}\right)}{2A^{3/2}} \tag{A24}$$

$$\mathrm{Res}\left\{e^{-\mathrm{i}\omega t}E(t),t_2\right\} = -\frac{e^{-\frac{\omega}{2}\left(1+q_2-\mathrm{i}\sqrt{A}\right)}\omega\rho\left(2\mathrm{i}+\omega\sqrt{A}\right)}{2A^{3/2}} \tag{A25}$$

For $\omega = 0$, the choice of the contour does not alter the result and knowing that there are no poles in the upper half plane and the line of real values, the calculus of residues gives immediately the answer of having a zero integral. That is, there are no dc components in the field.

Finally, the Fourier transform for the TE "1-cycle" pulse is given by the equation

$$E_{\mathrm{re}}(\omega) = \begin{cases} \left\{\mathrm{i}\pi\omega\rho e^{-\frac{\omega(q_2+1)}{2}}\frac{e^{\frac{\mathrm{i}\omega}{2}\sqrt{A}}\left(2\mathrm{i}+\omega\sqrt{A}\right)+e^{-\frac{\mathrm{i}\omega}{2}\sqrt{A}}\left(-2\mathrm{i}+\omega\sqrt{A}\right)}{2A^{3/2}}\right\}^* & \omega > 0 \\ \mathrm{i}\pi\omega\rho e^{\frac{\omega(q_2+1)}{2}}\frac{e^{-\frac{\omega\mathrm{i}}{2}\sqrt{A}}\left(-2\mathrm{i}+\omega\sqrt{A}\right)+e^{\frac{\omega\mathrm{i}}{2}\sqrt{A}}\left(2\mathrm{i}+\omega\sqrt{A}\right)}{2A^{3/2}} & \omega < 0 \\ 0 & \omega = 0 \end{cases} \tag{A26}$$

with

$$A \equiv A(\rho,z,q_2) = -(-1+q_2-2\rho-2\mathrm{i}z)(-1+q_2+2\rho-2\mathrm{i}z), \tag{A27}$$

which can be simplified to a single line, given that for the Fourier transform of a real function, it holds that $F(\omega) = F^*(-\omega)$.

It is now clear from Eq. (A6 - A8) that the magnetic fields satisfy the necessary conditions to apply Jordan's lemma and that they have the same poles with the electric field. Hence, the exact same approach can be used leading to the following frequency domain expressions

for the magnetic field

$$H_{\rho,\mathrm{re}}(\omega)=\begin{cases}\left\{(q_2-1-2\mathrm{i}z)\,\pi\rho e^{\frac{-\omega(q_2+1)}{2}}\left(-\frac{e^{\frac{\omega\mathrm{i}}{2}\sqrt{A}}\left(-12+6\mathrm{i}\sqrt{A}\omega+A\omega^2\right)}{2A^{5/2}}\right.\right. & \\ \left.\left.+\frac{e^{\frac{-\omega\mathrm{i}}{2}\sqrt{A}}\left(-12-6\mathrm{i}\sqrt{A}\omega+A\omega^2\right)}{2A^{5/2}}\right)\right\}^* & \omega>0\\ (q_2-1-2\mathrm{i}z)\,\pi\rho e^{\frac{\omega(q_2+1)}{2}}\left(-\frac{e^{-\frac{\omega\mathrm{i}}{2}\sqrt{A}}\left(-12-6\mathrm{i}\sqrt{A}\omega+A\omega^2\right)}{2A^{5/2}}\right. & \\ \left.+\frac{e^{\frac{\omega\mathrm{i}}{2}\sqrt{A}}\left(-12+6\mathrm{i}\sqrt{A}\omega+A\omega^2\right)}{2A^{5/2}}\right) & \omega<0\\ 0 & \omega=0\end{cases}\tag{A28}$$

$$H_{z,\mathrm{re}}(\omega)=\begin{cases}\left\{-\pi\mathrm{i}e^{\frac{-\omega(q_2+1)}{2}}\left(\frac{e^{\frac{\omega\mathrm{i}}{2}\sqrt{A}}\left(Ar^2\omega^2+(A-6r^2)(2-\mathrm{i}\sqrt{A}\omega)\right)}{A^{5/2}}\right.\right. & \\ \left.\left.+\frac{e^{-\frac{\omega\mathrm{i}}{2}\sqrt{A}}\left(-Ar^2\omega^2+(A-6r^2)(-2-\mathrm{i}\sqrt{A}\omega)\right)}{A^{5/2}}\right)\right\}^* & \omega>0\\ -\pi\mathrm{i}e^{\frac{\omega(q_2+1)}{2}}\left(\frac{e^{-\frac{\omega\mathrm{i}}{2}\sqrt{A}}\left(Ar^2\omega^2+(A-6r^2)(2+\mathrm{i}\sqrt{A}\omega)\right)}{A^{5/2}}\right. & \\ \left.+\frac{e^{\frac{\omega\mathrm{i}}{2}\sqrt{A}}\left(-Ar^2\omega^2+(A-6r^2)(-2+\mathrm{i}\sqrt{A}\omega)\right)}{A^{5/2}}\right) & \omega<0\\ 0 & \omega=0\end{cases}\tag{A29}$$

Of course one has to return to dimensional variables and insert the omitted coefficient in order to have the actual fields as follows

$$E_{\mathrm{re}}(\omega)=\begin{cases}4f_0\sqrt{\mu_0/\epsilon_0}\left\{\mathrm{i}\pi\frac{\omega}{c^2}\frac{\rho}{q_1}e^{-\frac{\omega(q_2+q_1)}{2c}}\frac{e^{\frac{\mathrm{i}\omega}{2c}\sqrt{A}}\left(2c\mathrm{i}+\omega\sqrt{A}\right)+e^{-\frac{\mathrm{i}\omega}{2c}\sqrt{A}}\left(-2c\mathrm{i}+\omega\sqrt{A}\right)}{2A^{3/2}}\right\}^* & \omega>0\\ 4f_0\sqrt{\mu_0/\epsilon_0}\mathrm{i}\pi\frac{\omega}{c^2}\frac{\rho}{q_1}e^{\frac{\omega(q_2+q_1)}{2c}}\frac{e^{-\frac{\omega\mathrm{i}}{2c}\sqrt{A}}\left(-2c\mathrm{i}+\omega\sqrt{A}\right)+e^{\frac{\omega\mathrm{i}}{2c}\sqrt{A}}\left(2c\mathrm{i}+\omega\sqrt{A}\right)}{2A^{3/2}} & \omega<0\\ 0 & \omega=0\end{cases}\tag{A30}$$

$$H_{\rho,\mathrm{re}}(\omega)=\begin{cases}\left\{4f_0\pi\rho\frac{(q_2-q_1-2\mathrm{i}z)}{q_1c^2}e^{\frac{-\omega(q_2+q_1)}{2c}}\left(-\frac{e^{\frac{\omega\mathrm{i}}{2c}\sqrt{A}}\left(-12c^2+6\mathrm{i}\sqrt{A}\omega c+A\omega^2\right)}{2A^{5/2}}\right.\right. & \\ \left.\left.+\frac{e^{\frac{-\omega\mathrm{i}}{2c}\sqrt{A}}\left(-12c^2-6\mathrm{i}\sqrt{A}\omega c+A\omega^2\right)}{2A^{5/2}}\right)\right\}^* & \omega>0\\ 4f_0\pi\rho\frac{(q_2-q_1-2\mathrm{i}z)}{q_1c^2}e^{\frac{\omega(q_2+q_1)}{2c}}\left(-\frac{e^{-\frac{\omega\mathrm{i}}{2c}\sqrt{A}}\left(-12c^2-6\mathrm{i}\sqrt{A}\omega c+A\omega^2\right)}{2A^{5/2}}\right. & \\ \left.+\frac{e^{\frac{\omega\mathrm{i}}{2c}\sqrt{A}}\left(-12c^2+6\mathrm{i}\sqrt{A}\omega c+A\omega^2\right)}{2A^{5/2}}\right) & \omega<0\\ 0 & \omega=0\end{cases}\tag{A31}$$

$$H_{z,\mathrm{re}}(\omega)=\begin{cases}\left\{-\frac{4\pi\mathrm{i}f_0}{q_1c}e^{\frac{-\omega(q_2+q_1)}{2c}}\left(\frac{e^{\frac{\omega\mathrm{i}}{2c}\sqrt{A}}\left(Ar^2\omega^2/c+(A-6r^2)(2c-\mathrm{i}\sqrt{A}\omega)\right)}{A^{5/2}}\right.\right. & \\ \left.\left.+\frac{e^{\frac{-\omega\mathrm{i}}{2c}\sqrt{A}}\left(-Ar^2\omega^2/c+(A-6r^2)(-2c-\mathrm{i}\sqrt{A}\omega)\right)}{A^{5/2}}\right)\right\}^* & \omega>0\\ -\frac{4\pi\mathrm{i}f_0}{q_1c}e^{\frac{\omega(q_2+q_1)}{2c}}\left(\frac{e^{-\frac{\omega\mathrm{i}}{2c}\sqrt{A}}\left(Ar^2\omega^2/c+(A-6r^2)(2c+\mathrm{i}\sqrt{A}\omega)\right)}{A^{5/2}}\right. & \\ \left.+\frac{e^{\frac{\omega\mathrm{i}}{2c}\sqrt{A}}\left(-Ar^2\omega^2/c+(A-6r^2)(-2c+\mathrm{i}\sqrt{A}\omega)\right)}{A^{5/2}}\right) & \omega<0\\ 0 & \omega=0\end{cases}\tag{A32}$$

with

$$A\equiv A(\rho,z,q_2)=-(-q_1+q_2-2\rho-2\mathrm{i}z)(-q_1+q_2+2\rho-2\mathrm{i}z).\tag{A33}$$

Because now of the analyticity of the Eq. (A3-A5), with respect to time, the real and imaginary parts (or equivalently the "1-cycle" and "$1\frac{1}{2}$-cycle") form Hilbert transform pairs, which means that they share the same spectrum with a change only in phase, as it is clear from the following relations, [11, 24]

$$\mathbf{E}_{\mathrm{im}}(\omega)=\mathrm{i}\,\mathrm{sgn}(\omega)\mathbf{E}_{\mathrm{re}}(\omega)\tag{A34}$$

and

$$\mathbf{H}_{\mathrm{im}}(\omega)=\mathrm{i}\,\mathrm{sgn}(\omega)\mathbf{H}_{\mathrm{re}}(\omega),\tag{A35}$$

with

$$\mathrm{sgn}(\omega) = \begin{cases} 1, & \omega > 0 \\ -1, & \omega < 0 \\ 0, & \omega = 0 \end{cases} . \tag{A36}$$

Finally, regarding the TM pulses, the frequency domain equations can be derived by a substitution of the TE formulas to the following equations

$$\mathbf{E}_{\mathrm{TM}} = \sqrt{\frac{\mu_0}{\epsilon_0}}\mathbf{H}_{\mathrm{TE}} \tag{A37}$$

$$\mathbf{H}_{\mathrm{TM}} = -\sqrt{\frac{\epsilon_0}{\mu_0}}\mathbf{E}_{\mathrm{TE}}. \tag{A38}$$

Appendix B: Proof of isodiffraction for well-collimated Donut pulses

We now prove that in the paraxial regime of well-collimated pulses, $q_2 \gg q_1$, the FD pulse is isodiffracting. We show that, far from the focus, in each cross-section of the beam perpendicular to the direction of propagation the spatial profiles of intensity for every frequency component of the beam scales along the trajectory of the beam in the same way. This is achieved by tracing the radial position of the maxima of each spectral component $\rho_{\max}(\omega)$ and showing that the ratio of these radial positions between any two monochromatic beams is independent of the propagation distance z, $\rho_{\max}(\omega_2)/\rho_{\max}(\omega_1) = \text{const}$, and that smaller wavelengths are always closer to the center of the beam. We finally derive an approximate expression for the divergence angle of each spectral component where we show that it is proportional to the square root of its wavelength. A comparison with the divergence angle of Gaussian beams shows that such dependence corresponds to isodiffracting beams and thus all spectral components of the FD share the same Rayleigh length that it is shown to be proportional to q_2.

Since the spectrum is symmetric with respect to the $z = 0$ plane, which is the focal plane we can prove the isodiffracting property of the pulse for $z > 0$ without loss of generality. The same is true for ω and hence we restrict our analysis to $z > 0$ and $\omega > 0$. It turns out

that in this case the Fourier transform of the pulse is simplified to the following equation

$$E^*_{\rm re}(\omega) = {\rm i}\pi\omega\rho e^{-\frac{\omega(q_2+1)}{2}} \frac{e^{-\frac{{\rm i}\omega}{2}\sqrt{A}}\left(-2{\rm i}+\omega\sqrt{A}\right)}{2A^{3/2}}. \tag{B1}$$

That is because $\mathrm{Im}\left\{\sqrt{A}\right\} > 0$ and hence the positive exponential of Eq. A30

$$e^{\frac{{\rm i}\omega}{2}\sqrt{A}} = e^{\frac{{\rm i}\omega}{2}\mathrm{Re}\left\{\sqrt{A}\right\}} e^{\frac{-\omega}{2}\mathrm{Im}\left\{\sqrt{A}\right\}} \tag{B2}$$

is negligible compared to the negative exponential

$$e^{\frac{-{\rm i}\omega}{2}\sqrt{A}} = e^{-\frac{{\rm i}\omega}{2}\mathrm{Re}\left\{\sqrt{A}\right\}} e^{\frac{\omega}{2}\mathrm{Im}\left\{\sqrt{A}\right\}} \tag{B3}$$

and thus it can be ignored. The spectrum of the electric field is now given by the following equation

$$\begin{aligned} I_{\rm re}(\omega) &= E_{\rm re}(\omega)E^*_{\rm re}(\omega) \\ &= \pi^2\omega^2\rho^2 e^{-\omega(q_2+1)} \frac{e^{\omega\mathrm{Im}\left\{\sqrt{A}\right\}}\left(4-4\omega\mathrm{Im}\left\{\sqrt{A}\right\}+\omega|A|\right)}{2|A|^3}. \end{aligned} \tag{B4}$$

For $z \gg q_2$ we can write

$$|A| = 4(z^2+\rho^2) \tag{B5}$$

and

$$\begin{aligned} \mathrm{Im}\left\{\sqrt{A}\right\} &= \sqrt{|A|}\sin\left[\frac{1}{2}\mathrm{Arg}\,(A)\right] \\ &= \sqrt{|A|}\sin\left[\frac{1}{2}\arctan\left(\frac{4(q_2-1)z}{4z^2+4\rho^2-(q_2-1)^2}\right)\right] \\ &= \frac{(q_2-1)z}{\sqrt{z^2+\rho^2}} \end{aligned} \tag{B6}$$

since $\sin(x) \simeq x$ and $\arctan(x) \simeq x$ for $x \ll 1$. In addition $|A| \gg \mathrm{Im}\left\{\sqrt{A}\right\}$ and $|A| \gg 4$

leading to a simplified expression for the spectrum in the far field

$$I_{\mathrm{re}}(\omega) = \pi^2\omega^3\rho^2 e^{-\omega(q_2+1)} \frac{e^{\frac{\omega(q_2-1)z}{\sqrt{z^2+\rho^2}}}}{32(z^2+\rho^2)^2}. \tag{B7}$$

The general shape of the spectrum is the same for any frequency and propagation distance since it is given by the same equation. This equation has only one extrema which is the maximum of the intensity. That is easy to see since the function is actually the product of a decreasing exponential with the ratio of a second degree parabola and a shifted fourth degree parabola. The ratio has only one maximum and the exponential is simply shifting this maximum in space. Hence we only have to find the position of this maximum. That is the zero of the derivative of the intensity with respect to the radius, $\frac{dI_{\mathrm{re}}(\omega,\rho)}{d\rho}|_{\rho_{\max}} = 0$, which is given by the solution of the following equation

$$4x^3 - (4+\omega^2(q_2-1)^2)z^2x^2 - 4z^4x + 4z^6 = 0 \tag{B8}$$

with $\rho_{\max} = \sqrt{x_0}$, where x_0 is the only real solution of Eq. B8. However in the paraxial case, the radial expansion of the beam increases with a much smaller rate than the propagation distance z. Hence the first term of the polynomial, $x^3 = \rho^6$, will be very small compared to the rest terms containing z and thus it can be ignored. Finally, the equation to be solved becomes

$$(4+\omega^2(q_2-1)^2)x^2 + 4z^2x - 4z^4 = 0 \tag{B9}$$

and the radial position of the maximum electric field amplitude for each spectral component in the far field is given by the following simple equation

$$\rho_{\max} = z\sqrt{\frac{-2+2\sqrt{5+(q_2-1)^2\omega^2}}{4+(q_2-1)^2\omega^2}}. \tag{B10}$$

The ratio of the radial position of the maxima between two different wavelengths is easily obtained as

$$\xi(\omega_2) = \frac{\rho_{\max}(\omega_2)}{\rho_{\max}(\omega_1)} = \sqrt{\frac{(4+(q_2-1)^2\omega_1^2)(-2+2\sqrt{5+(q_2-1)^2\omega_2^2})}{(-2+2\sqrt{5+(q_2-1)^2\omega_1^2})(4+(q_2-1)^2\omega_2^2)}} \tag{B11}$$

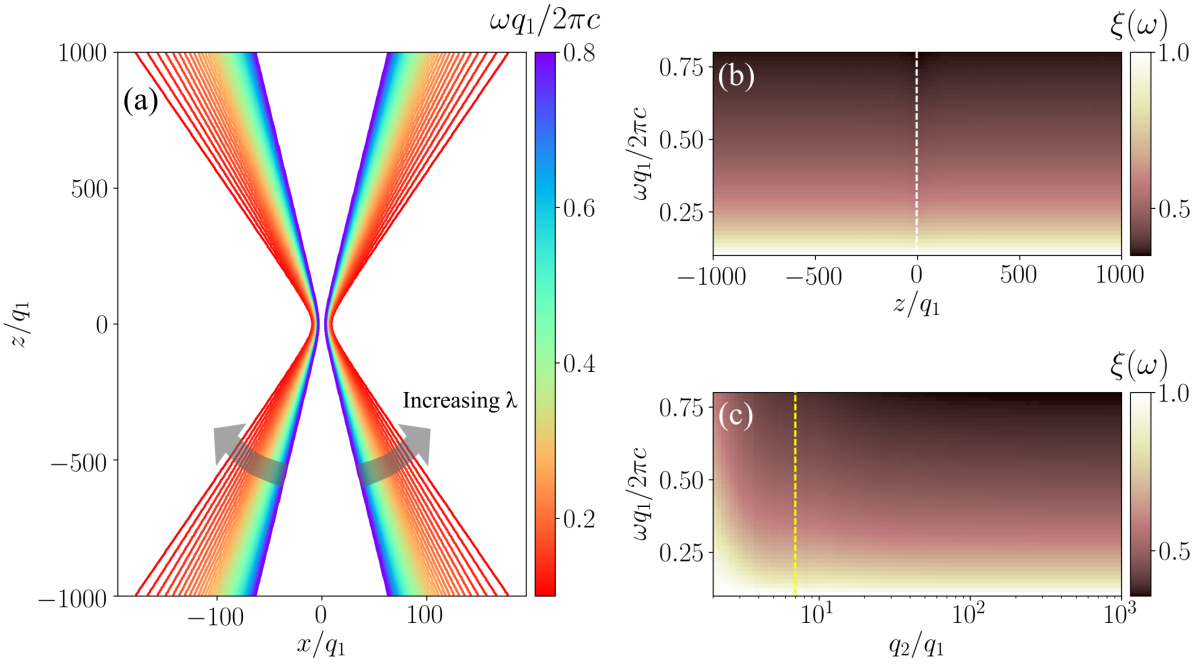

FIG. 6. (a) Trace of the position of the maximum intensity for each wavelength. (b) Numerical calculation of the dimensionless ratio of the radial position of the maxima between a reference frequency, $\omega_1 q_1/2\pi c = 0.1$ and a variable frequency ω, for $q_2 = 100q_1$ and for increasing propagation distance z/q_1. The white dashed line indicates the position of the focus. (c) Numerical calculation of the same ratio for fixed distance, $z/q_1 = 1000$ and for increasing q_2. For $z \gg q_2$ and $q_2 \gg q_1$ the value of the ratio is similar to the theoretically predicted value from Eq. B11. The yellow dashed line indicates the limit of q_2/q_1 below which Eq. B11 deviates from the actual value.

and is independent of the propagation distance z. In addition it is easy to prove that Eq. B10 is a monotonically decreasing function of ω.

To illustrate the validity of Eq. B11, we plot the radial position of the maximum intensity of the FD pulse for each wavelength and increasing propagation distance z/q_1 with $q_2 = 100q_1$, Fig. 6a. Then we use as a reference frequency the smallest frequency on the plot, $\omega_1 q_1/2\pi c = 0.1$ and calculate the ratio of the position of the maxima for all frequencies up to $\omega q_1/2\pi c = 0.8$, $\frac{\rho_{\max}(\omega)}{\rho_{\max}(\omega_1)}$. We do this for various values of propagation distance z/q_1, Fig. 6b, and parameter q_2, Fig. 6c. For $z \gg q_2$ and $q_2 \gg q_1$ the value of the ratio is similar to the theoretically predicted value from Eq. B11 verifying its validity. Additionally, we note that the ratio is always smaller than unity which indicates that the shorter wavelengths exhibit peak values of spectral intensity at smaller radii in accordance with Fig. 2c of the main text. As predicted by Eq. B11, away from focus the ratio is independent of the propagation

distance (see Fig. 6b). From Fig. 6b we also notice that the ratio ξ varies very little even at focus which is an indication that the FD pulse is isodiffracting. From Fig. 6c and for $q_2 \gg q_1$ we notice that the ratio becomes independent of the parameter q_2, meaning that for very well collimated beams the ratio of the position of the maxima between two frequencies can be described by a very simple expression that is proportional to the ratio of the frequencies.

Finally, Eq. B10 is true for $z \gg q_1$ and thus is appropriate for the calculation of the divergence angle of each beam. Since all our calculations are for the paraxial regime $q_2 \gg q_1$, the angle of divergence is small and can be given approximately as

$$\Theta_{\mathrm{div}} \simeq \arctan\left(\frac{\rho_{\max}}{z}\right) \simeq \sqrt{\frac{-2+2\sqrt{5+(q_2-1)^2\omega^2}}{4+(q_2-1)^2\omega^2}} \simeq \sqrt{\frac{2}{q_2\omega}}. \tag{B12}$$

The important thing to notice here is the similarity with the expression of the divergence angle of a Gaussian beam $\Theta_{\mathrm{div}} \simeq \sqrt{\lambda/z_{\mathrm{R}}\pi}$, where z_{R} is the Rayleigh length [25]. It is now clear that the parameter q_2 has the role of the Rayleigh length and since it does not depend on the wavelength the beams that compose the FD pulse are isodiffracting.

Appendix C: Hankel transform

By using Jordan's lemma in a similar way with App. A, an analytical expression for one of the spatial coordinates of the FD pulse can be derived. However, it is clear that the pulse does not depend on the polar angle θ. This symmetry can be exploited and a Hankel transform can be applied for the calculation of the spatial frequencies in a transverse plane r, θ [17]. In our case the intensity of the pulse is circularly invariant but the field is not. It has a polarization singularity at the center leading to a sign inversion of the field across a line passing through the center of the pulse.

In this appendix we derive a closed form expression for the Hankel transform of the electric field of the TE pulse. A similar analysis can be applied for the TM pulse. In order to deal with the polarization we start by projecting the $\hat{\boldsymbol{\theta}}$ dependence of the field to the $\hat{\boldsymbol{x}}$, $\hat{\boldsymbol{y}}$ plane. The following relations between Cartesian and polar coordinates will be used

$$\begin{aligned}
&\rho = \sqrt{x^2+y^2}, && \hat{\boldsymbol{\rho}} = \cos\theta\hat{\boldsymbol{x}} + \sin\theta\hat{\boldsymbol{y}} \\
&\theta = \arctan\left(\tfrac{y}{x}\right), && \hat{\boldsymbol{\theta}} = -\sin\theta\hat{\boldsymbol{x}} + \cos\theta\hat{\boldsymbol{y}} \\
&x = \rho\cos\theta, && \hat{\boldsymbol{x}} = \cos\theta\hat{\boldsymbol{\rho}} - \sin\theta\hat{\boldsymbol{\theta}} \\
&y = \rho\sin\theta, && \hat{\boldsymbol{y}} = \sin\theta\hat{\boldsymbol{\rho}} + \cos\theta\hat{\boldsymbol{\theta}}
\end{aligned} \tag{C1}$$

for the real space and

$$\begin{aligned}
&k_\rho = \sqrt{k_x^2+k_y^2}, && \hat{\boldsymbol{k}}_{\boldsymbol{\rho}} = \cos k_\theta\hat{\boldsymbol{k}}_{\boldsymbol{x}} + \sin k_\theta\hat{\boldsymbol{k}}_{\boldsymbol{y}} \\
&k_\theta = \arctan\left(\tfrac{k_y}{k_x}\right), && \hat{\boldsymbol{k}}_{\boldsymbol{\theta}} = -\sin k_\theta\hat{\boldsymbol{k}}_{\boldsymbol{x}} + \cos k_\theta\hat{\boldsymbol{k}}_{\boldsymbol{y}} \\
&k_x = k_\rho\cos k_\theta, && \hat{\boldsymbol{k}}_{\boldsymbol{x}} = \cos k_\theta\hat{\boldsymbol{k}}_{\boldsymbol{\rho}} - \sin k_\theta\hat{\boldsymbol{k}}_{\boldsymbol{\phi}} \\
&k_y = k_\rho\sin k_\theta, && \hat{\boldsymbol{k}}_{\boldsymbol{y}} = \sin k_\theta\hat{\boldsymbol{k}}_{\boldsymbol{\rho}} + \cos k_\theta\hat{\boldsymbol{k}}_{\boldsymbol{\phi}}
\end{aligned} \tag{C2}$$

for the k-space. From the above we have

$$\mathbf{E}(\rho,\theta) = -\sin\theta E_\theta(\rho)\,\hat{\boldsymbol{x}} + \cos\theta E_\theta(\rho)\,\hat{\boldsymbol{y}}. \tag{C3}$$

It is now clear that each polarization of the field is separable in the polar coordinates. In that case the Fourier transform can be expressed as an infinite sum of weighted Hankel transforms [17]. Let $\mathcal{F}$ and $\mathcal{H}$ denote the Fourier and Hankel transforms of a function respectively and $g(\rho,\theta) = g_\theta(\theta)g_\rho(\rho)$ being the separable function to be Fourier transformed. Then we can write

$$\mathcal{F}[g(\rho,\theta)] = \sum_{-\infty}^{\infty} c_m(-\mathrm{i})^m \mathrm{e}^{\mathrm{i}mk_\theta}\mathcal{H}_m[g_\rho(\rho)], \tag{C4}$$

with

$$c_m = \frac{1}{2\pi}\int_0^\infty g_\theta(\theta)\mathrm{e}^{-\mathrm{i}m\theta}d\theta, \tag{C5}$$

$$\mathcal{H}[g_\rho(\rho)] = 2\pi\int_0^\infty \rho g_\rho(\rho)J_m(k_\rho\rho)d\rho \tag{C6}$$

and J_m the m order Bessel function of the first kind. If the azimuthal part of the field $g_\theta(\theta)$ has some kind of azimuthal symmetry, as in our case, then only a few terms of the infinite

sum will contribute to the result making the problem tractable.

For the E_x component we have $g_\theta(\theta) = -\sin\theta$ and

$$c_m = \frac{-1}{2\pi}\int_0^{2\pi} \sin\theta \mathrm{e}^{-\mathrm{i}m\theta} d\theta = \frac{-1}{2\pi}\int_0^{2\pi} \frac{\mathrm{e}^{-\mathrm{i}\theta(m-1)}}{2\mathrm{i}} d\theta + \frac{1}{2\pi}\int_0^{2\pi} \frac{\mathrm{e}^{-\mathrm{i}\theta(m+1)}}{2\mathrm{i}} d\theta$$
$$= \begin{cases} -\frac{1}{2\mathrm{i}}, & m = 1 \\ \frac{1}{2\mathrm{i}}, & m = -1 \\ 0, & m \neq \pm 1 \end{cases} \tag{C7}$$

and for the E_y, $g_\theta(\theta) = \cos\theta$ and

$$c_m = \begin{cases} \frac{1}{2}, & m \pm 1 \\ 0, & m \neq \pm 1 \end{cases}. \tag{C8}$$

Hence, from Eq. (C3 - C8) and by using the identity $J_{-n}(x) = (-1)^n J_n(x)$ we have

$$E_x\left(k_\rho, k_\theta\right)\hat{\boldsymbol{x}} = 2\pi\mathrm{i}\sin k_\theta \int_0^\infty \rho E_\theta\left(\rho\right) J_1(k_\rho\rho) d\rho\hat{\boldsymbol{x}} \tag{C9}$$

and

$$E_y\left(k_\rho, k_\theta\right)\hat{\boldsymbol{y}} = -2\pi\mathrm{i}\cos k_\theta \int_0^\infty \rho E_\theta\left(\rho\right) J_1(k_\rho\rho) d\rho\hat{\boldsymbol{y}}. \tag{C10}$$

However, since $\hat{\boldsymbol{x}}, \hat{\boldsymbol{y}}, \hat{\boldsymbol{\theta}}, \hat{\boldsymbol{k}}_{\boldsymbol{x}}, \hat{\boldsymbol{k}}_{\boldsymbol{y}}$ and $\hat{\boldsymbol{k}}_{\boldsymbol{\theta}}$ are unit vectors in the same coordinate system, $\hat{\boldsymbol{x}} = \hat{\boldsymbol{k}}_{\boldsymbol{x}}$, $\hat{\boldsymbol{y}} = \hat{\boldsymbol{k}}_{\boldsymbol{y}}$ and $\hat{\boldsymbol{\theta}} = \hat{\boldsymbol{k}}_{\boldsymbol{\theta}}$ leading to a single azimuthally polarized equation without a k_θ dependence

$$\mathbf{E}\left(k_\rho\right) = -2\pi\mathrm{i}\int_0^\infty \rho E_\theta\left(\rho\right) J_1(k_\rho\rho) d\rho\hat{\boldsymbol{\theta}}. \tag{C11}$$

For the inverse transform we have to look first at the definition of the forward transform that was used to derive Eq. C11,

$$\mathbf{E}\left(k_\rho, k_\theta\right) = \int_0^{2\pi}\int_0^\infty -\sin\theta \mathrm{e}^{-ik_\rho\rho(\cos\theta\cos k_\theta + \sin\theta\sin k_\theta)} E_\theta\left(\rho\right) \rho d\rho d\theta\hat{\boldsymbol{x}}$$
$$+ \int_0^{2\pi}\int_0^\infty \cos\theta \mathrm{e}^{-ik_\rho\rho(\cos\theta\cos k_\theta + \sin\theta\sin k_\theta)} E_\theta\left(\rho\right) \rho d\rho d\theta\hat{\boldsymbol{y}}. \tag{C12}$$

In the same manner we can write the inverse as

$$\mathbf{E}\left(\rho,\theta\right)=\frac{1}{4\pi^2}\int_0^{2\pi}\int_0^{\infty}-\sin k_\theta \mathrm{e}^{ik_\rho\rho(\cos\theta\cos k_\theta+\sin\theta\sin k_\theta)}E_\theta\left(k_\rho\right)k_\rho dk_\rho dk_\theta\hat{\boldsymbol{k}}_{\boldsymbol{x}}$$
$$+\frac{1}{4\pi^2}\int_0^{2\pi}\int_0^{\infty}\cos k_\theta \mathrm{e}^{ik_\rho\rho(\cos\theta\cos k_\theta+\sin\theta\sin k_\theta)}E_\theta\left(k_\rho\right)k_\rho dk_\rho dk_\theta\hat{\boldsymbol{k}}_{\boldsymbol{y}}. \tag{C13}$$

Finally, we define $\theta'=\theta-\pi$, hence $\sin(\theta'+\pi)=-\sin\theta'$ and $\cos(\theta'+\pi)=-\cos\theta'$. The integral limits change to $(-\pi,\pi)$ but since the integrand has a period of 2π this does not change the integral and hence there is no need to change the limits. By ignoring the prime at θ' for clarity we end up with the following equation for the inverse Fourier transform

$$\mathbf{E}\left(\rho,\theta\right)=\frac{1}{4\pi^2}\int_0^{2\pi}\int_0^{\infty}\sin k_\theta \mathrm{e}^{-ik_\rho\rho(\cos\theta\cos k_\theta+\sin\theta\sin k_\theta)}E_\theta\left(k_\rho\right)k_\rho dk_\rho dk_\theta\hat{\boldsymbol{k}}_{\boldsymbol{x}}$$
$$+\frac{1}{4\pi^2}\int_0^{2\pi}\int_0^{\infty}-\cos k_\theta \mathrm{e}^{-ik_\rho\rho(\cos\theta\cos k_\theta+\sin\theta\sin k_\theta)}E_\theta\left(k_\rho\right)k_\rho dk_\rho dk_\theta\hat{\boldsymbol{k}}_{\boldsymbol{y}}. \tag{C14}$$

It is now clear that by swapping ρ with k_ρ and θ with k_θ, Eq. C14 is identical to Eq. C12 with the exception of the coefficient $\frac{1}{4\pi^2}$ and a minus sign. Hence the inverse Fourier transform can be given from the following Hankel transform

$$\mathbf{E}\left(\rho\right)=\frac{\mathrm{i}}{2\pi}\int_0^{\infty}k_\rho E_\theta\left(k_\rho\right)J_1(k_\rho\rho)dk_\rho\hat{\boldsymbol{\theta}}. \tag{C15}$$

Returning to Eq. C11, we will solve the integral for the complex expression of the field. The transforms of the real and imaginary fields are then simply taken from the following equations

$$E_{\mathrm{re},\theta}(k_\rho)=\frac{E_\theta(k_\rho)-E_\theta^*(k_\rho)}{2} \tag{C16}$$
$$E_{\mathrm{im},\theta}(k_\rho)=\frac{E_\theta(k_\rho)+E_\theta^*(k_\rho)}{2\mathrm{i}}. \tag{C17}$$

Proof.

$$\begin{aligned} E_{\mathrm{re},\theta}(k_\rho) &= -2\pi\mathrm{i}\int_0^\infty \mathrm{Re}\left\{E_\theta(\rho)\right\} J_1(k_\rho\rho)\rho d\rho \\ &= \int_0^\infty \frac{-2\pi\mathrm{i}E_\theta(\rho)}{2} J_1(k_\rho\rho)\rho d\rho - \left[\int_0^\infty \frac{-2\pi\mathrm{i}E_\theta(\rho)}{2} J_1(k_\rho\rho)\rho d\rho\right]^* \\ &= \frac{E_\theta(k_\rho) - E_\theta^*(k_\rho)}{2} \end{aligned}$$

and similar for the imaginary part, given that k_ρ and ρ are real. □

For clarity we rewrite the electric field expression as follows

$$\begin{aligned} E_\theta &= -4\mathrm{i}f_0\sqrt{\frac{\mu_0}{\epsilon_0}}\frac{\rho\left(q_1+q_2-2\mathrm{i}ct\right)}{\left[\rho^2+(q_1+\mathrm{i}z-\mathrm{i}ct)(q_2-\mathrm{i}z-\mathrm{i}ct)\right]^3} \\ &= \mathrm{coef}\frac{\rho}{\left(\rho^2+\alpha^2\right)^3} \end{aligned} \tag{C18}$$

with $coef = -4\mathrm{i}f_0\sqrt{\frac{\mu_0}{\epsilon_0}}(q_1+q_2-2\mathrm{i}ct)$ and $\alpha = \sqrt{(q_1+\mathrm{i}z-\mathrm{i}ct)(q_2-\mathrm{i}z-\mathrm{i}ct)}$. The integral that we have to solve now becomes

$$E_\theta(k_\rho) = -2\pi\mathrm{i}coef\int_0^\infty \frac{\rho^2}{\left(\rho^2+\alpha^2\right)^3} J_1(k_\rho\rho)d\rho. \tag{C19}$$

The solution of an integral of the above form is known when it satisfies some criteria and it is given from the following form [26, 27]

$$\int_0^\infty \frac{\rho^{\nu+1}}{(\rho^2+\alpha^2)^{\mu+1}} J_\nu(k\rho)d\rho = \frac{k^\mu\alpha^{\nu-\mu}}{2^\mu\Gamma(\mu+1)} K_{\nu-\mu}(k\alpha) \tag{C20}$$

with $\mathrm{Re}\left\{\alpha\right\} > 0$ and $-1 < \mathrm{Re}\left\{\nu\right\} < 2\mathrm{Re}\left\{\mu\right\} + 3/2$. K_ν is the ν order modified Bessel function of the second kind and Γ denotes the Gamma function with its integral definition being [23]

$$\Gamma(z) = \int_0^\infty t^{z-1}e^t dt,\ \mathrm{Re}\left\{z\right\} > 0. \tag{C21}$$

The only properties of this function that we will need here are

$$\Gamma(z+1) = z\Gamma(z), \tag{C22}$$

$$\Gamma(1) = 1. \tag{C23}$$

In our case, $\nu = 1$ and $\mu = 2$ and hence the second criterion is satisfied. The first criterion requires $\mathrm{Re}\{\alpha\} > 0$ or $|\arg(\alpha)| < \pi/2$. We will now show that $|\arg(\alpha)| < \pi/2$ is true in our case and hence all the conditions needed to apply the above formula are met.

Proof. We have,

$$\alpha = \sqrt{q_1 q_2 + z^2 - c^2 t^2 - \mathrm{i}\left(ct(q_1+q_2) + z(q_1-q_2)\right)}$$
$$\beta = \alpha^2 = q_1 q_2 + z^2 - c^2 t^2 - \mathrm{i}\left(ct(q_1+q_2) + z(q_1-q_2)\right).$$

We want to study when $|\arg(\alpha)| < \pi/2$ or, since $\alpha = \sqrt{\beta} = \sqrt{|\beta|e^{\mathrm{i}\theta}} = \sqrt{|\beta|}e^{\mathrm{i}\theta/2}$, when $|\arg(\beta)| = |\arg(\alpha^2)| < \pi$. We write $\beta = x + y\mathrm{i}$ and hence $\arg(\beta) = \mathrm{atan2}(y, x)$. From Eq. A15 there is only one case that the criterion can be possibly violated, the case $\arctan(y/x)+\pi$ with $x < 0, y \geq 0$. But $-\pi/2 < \arctan(y/x) \leq 0$ and hence the equality $|\arg(\alpha)| = \pi/2$ can only happen when $y = 0$ and $x < 0$.

For $y = 0$ we have

$$ct = \frac{q_2 - q_1}{q_2 + q_1} z. \tag{C24}$$

For $x < 0$ we have

$$c^2 t^2 > q_1 q_2 + z^2. \tag{C25}$$

Substitution of Eq. C24 to C25 leads to the following statement

$$\frac{-4q_1 q_2}{(q_1+q_2)^2} z^2 > q_1 q_2 \tag{C26}$$

which is not true since q_1 and q_2 are both positive numbers. Hence, $|\arg(\alpha)|$ is always smaller than $\pi/2$. □

The Hankel transform is now given by the equation

$$E_\theta(k_\rho) = -2\pi \mathrm{i} coef \frac{k_\rho^2}{8\alpha} K_{-1}(k_\rho \alpha). \tag{C27}$$

From the definition of the K_ν it can be easily shown that $K_{-1}(x) = K_1(x)$, hence we finally have

$$\mathbf{E}(k_\rho) = -\pi f_0 \sqrt{\frac{\mu_0}{\epsilon_0}} (q_1 + q_2 - 2\mathrm{i}ct) \frac{k_\rho^2}{\alpha} K_1(k_\rho \alpha) \hat{\boldsymbol{\theta}}, \tag{C28}$$

with $\alpha = \sqrt{(q_1 + \mathrm{i}z - \mathrm{i}ct)(q_2 - \mathrm{i}z - \mathrm{i}ct)}$.

Finally, an alternative route for this derivation can be followed by starting from the definition of the scalar function f, Eq. 3. This function can be written as a superposition of bidirectional waves [20] that are solutions of the scalar wave equation and their integral representation directly leads to an integral for the Hankel transform of the fields.

---

[1] R. W. Hellwarth and P. Nouchi, "Focused one-cycle electromagnetic pulses," Phys. Rev. E **54**, 889–895 (1996).

[2] Apostolos Zdagkas, Nikitas Papasimakis, Vassili Savinov, Mark R. Dennis, and Nikolay I. Zheludev, "Singularities in the flying electromagnetic doughnuts," Nanophotonics **8**, 1379 – 1385 (2019).

[3] Tim Raybould, Vassili Fedotov, Nikitas Papasimakis, Ian Youngs, and Nikolay Zheludev, "Focused electromagnetic doughnut pulses and their interaction with interfaces and nanostructures," Opt. Express **24**, 3150–3161 (2016).

[4] N Papasimakis, VA Fedotov, V Savinov, TA Raybould, and NI Zheludev, "Electromagnetic toroidal excitations in matter and free space," Nature materials **15**, 263 (2016).

[5] Tim Raybould, Vassili A. Fedotov, Nikitas Papasimakis, Ian Youngs, and Nikolay I. Zheludev, "Exciting dynamic anapoles with electromagnetic doughnut pulses," Applied Physics Letters **111**, 081104 (2017), http://dx.doi.org/10.1063/1.4999368.

[6] James Neill Brittingham, "Focus wave modes in homogeneous maxwell's equation-te mode," *Journal of Applied Physics*, **54**, 1179 – 1189 (1983).

[7] Tai T. Wu and Ronold W. P. King, "Comment on "focus wave modes in homogeneous maxwell's equations: Transverse electric mode"," Journal of Applied Physics **56**, 2587–2588 (1984), http://dx.doi.org/10.1063/1.334289.

[8] Richard W Ziolkowski, "Localized transmission of electromagnetic energy," Physical Review A **39**, 2005 (1989).

[9] Richard W Ziolkowski, "Exact solutions of the wave equation with complex source locations," Journal of Mathematical Physics **26**, 861–863 (1985).

[10] Simin Feng, Herbert G. Winful, and Robert W. Hellwarth, "Gouy shift and temporal reshaping of focused single-cycle electromagnetic pulses," Opt. Lett. **23**, 385–387 (1998).

[11] Simin Feng, Herbert G. Winful, and Robert W. Hellwarth, "Spatiotemporal evolution of focused single-cycle electromagnetic pulses," Phys. Rev. E **59**, 4630–4649 (1999).

[12] Richard W. Ziolkowski, D. Kent Lewis, and Bill D. Cook, "Evidence of localized wave transmission," Phys. Rev. Lett. **62**, 147–150 (1989).

[13] Richard W. Ziolkowski and D. Kent Lewis, "Verification of the localized-wave transmission effect," Journal of Applied Physics **68**, 6083–6086 (1990), http://dx.doi.org/10.1063/1.346896.

[14] Hugo E Hernández-Figueroa, Michel Zamboni-Rached, and Erasmo Recami, *Non-diffracting waves* (John Wiley & Sons, 2013).

[15] Nikitas Papasimakis, Tim Raybould, Vassili A. Fedotov, Din Ping Tsai, Ian Youngs, and Nikolay I. Zheludev, "Pulse generation scheme for flying electromagnetic doughnuts," Phys. Rev. B **97**, 201409 (2018).

[16] Apostolos Zdagkas, Nikitas Papasimakis, Venkatram Nalla, Huifang Zhang, Oleksandr Buchnev, and Nikolai Zheludev, "Generation of electromagnetic doughnut pulses with a singular metamaterial converter," (2019).

[17] J.W. Goodman, *Introduction to Fourier Optics*, McGraw-Hill physical and quantum electronics series (W. H. Freeman, 2005).

[18] J. D. Jackson, *Classical Electrodynamics* (Wiley, New York ed. 3, 1999).

[19] Andrew W. Norfolk and Edward J. Grace, "Reconstruction of optical fields with the quasi-discrete hankel transform," Opt. Express **18**, 10551–10556 (2010).

[20] Ioannis M Besieris, Amr M Shaarawi, and Richard W Ziolkowski, "A bidirectional traveling plane wave representation of exact solutions of the scalar wave equation," Journal of Mathematical Physics **30**, 1254–1269 (1989).

[21] Rod Donnelly and Richard Ziolkowski, "A method for constructing solutions of homogeneous partial differential equations: localized waves," Proceedings of the Royal Society of London. Series A: Mathematical and Physical Sciences **437**, 673–692 (1992).

[22] Rod Donnelly and Richard W Ziolkowski, "Designing localized waves," Proceedings of the Royal Society of London. Series A: Mathematical and Physical Sciences **440**, 541–565 (1993).

[23] G.B. Arfken, H.J. Weber, and F.E. Harris, *Mathematical Methods for Physicists: A Comprehensive Guide* (Elsevier, 2012).

[24] Frederick W. King, *Hilbert Transforms*, Encyclopedia of Mathematics and its Applications, Vol. 1 (Cambridge University Press, 2009).

[25] Bahaa E A Saleh and Malvin Carl Teich, *Fundamentals of photonics; 2nd ed.*, Wiley series in pure and applied optics (Wiley, New York, NY, 2007).

[26] Qiong-Gui Lin, "Infinite integrals involving bessel functions by an improved approach of contour integration and the residue theorem," The Ramanujan Journal **35**, 443–466 (2014).

[27] G.N. Watson, *A Treatise on the Theory of Bessel Functions* (Cambridge University Press, 1944).